Performances of the Lamb Model to Describe the Vibrations of Gold Quantum-Sized Clusters

Quentin Martinet, Alice Berthelot, Adrien Girard, Baira Donoeva, Clothilde Comby-Zerbino, Élodie Romeo, Franck Bertorelle, Marte van Der Linden, Nathalie Tarrat, Nicolas Combe, et al.

Performances of the Lamb Model to Describe the Vibrations of Gold Quantum-sized Clusters

Quentin Martinet,[†,‡,¶] *Alice Berthelot,*[†,‡] *Adrien Girard,*[‡] *Baira Donoeva,*[‖] *Clothilde Comby-Zerbino,*[†] *Elodie Romeo,*[†] *Franck Bertorelle,*[†] *Marte van der Linden,*[‖] *Nathalie Tarrat,*[§] *Nicolas Combe* [§] *and Jérémie Margueritat*[†]

† Institut Lumière Matière, Université de Lyon, Université Claude Bernard Lyon 1, UMR CNRS 5306, 69622 Villeurbanne, France.

‡ Sorbonne Université, CNRS, De la Molécule aux Nano-objets : Réactivité, Interactions et Spectroscopies, MONARIS, F-75005 Paris, France.

‖ Inorganic Chemistry and Catalysis, Debye Institute for Nanomaterials Science, Utrecht University, Universiteitsweg 99, 3584 CG Utrecht, The Netherlands, 4ID26.

§ CEMES, Université de Toulouse, CNRS, 29, rue Jeanne Marvig, 31055 Toulouse, France.

KEYWORDS: nanomechanics, gold thiolate cluster, acoustic vibration, low frequency Raman spectroscopy, density functional theory computation.

ABSTRACT: Lamb modes describe the vibrations of an object as a whole from the stellar scale to the nanometer one. Lamb description has been built from the linear elasticity theory and considers a homogeneous elastic sphere. Our work tries to determine the minimum scale where this description remains valid by studying the vibration of quantum sized gold clusters (Au_6, Au_9 and Au_{25}) stabilized by organic molecules. First, our work shows that experimental frequencies of small functionalized gold clusters obtained using Low Frequency Raman Spectroscopy (LFRS) can be interpreted with density-functional theory (DFT) calculations. Moreover, the Lamb model broadly succeeds in predicting these Raman acoustic modes only if a correction considering the mass of the surrounding ligands is added. Ligands affect vibration modes of the core by their mass but also by their covalent bond with the core. The unexpected consequence of this electronic stabilization by the ligands is the sustainability of the Lamb description for clusters as small as 6 atoms. Finally, the limit of the Lamb model can be reached out at low temperature, where the vibration modes spectrum presents a sub-structuration that the Lamb description, developed for a homogeneous sphere, is unable to predict.

Introduction

Nanoscience has been an active research field from the discovery of the size dependence of structural[1], electronic[2], thermodynamic[3] and chemical properties[4]. Nanoparticles present original characteristics differing from the bulk material ones due to the electronic confinement and a high ratio of atoms at the surface with different valence states. Nanoparticles are of great interest in the fields of fundamental sciences and technological applications, due to the size tunability of their properties[5]. The general dependence of particle properties with size is separated into two scales. For large nanoparticles, there is a smooth variation from bulk values and for smaller nanoparticles, clusters, an irregular dependence due to the existence of magic numbers enhancing the electronic

stability[6,7]. By downsizing a nano-object, some particular effects could occur such as the modification or the disappearance of the localized surface Plasmon Resonance in small metallic cluster[8,9]. Moreover, atomic clusters clearly present different properties from isolated atoms due to the interatomic interactions[10]. Investigations have been performed on this latter size range in order to study the transition from condensed matter physics to a molecular description[11]. Vibrational spectroscopy, based on the study of vibrational modes, is a powerful tool to probe this transition. Due to the finite size of the object, the phonon waves are confined and a transition is observed in the vibrational spectrum of the nanoparticle from a continuous phonon dispersion, characteristic of the solid[12], to a discrete distribution of modes. The frequencies of these modes, first calculated by Sir Horace Lamb for a free homogeneous elastic sphere within the framework of the continuum mechanics, are inversely proportional to the diameter of the object[13,14]. Other theoretical work[15], based on atomistic stimulation, showed that in the range between Au_{766} and Au_{75}, continuum mechanics remains still surprisingly accurate, this latter being much more arguable in the range Au_4-Au_{25}[16]. Many experiments using Time Resolved Spectroscopy (TRS)[17–21] or Low Frequency Raman Spectroscopy (LFRS)[22–24] have been performed to test the validity of the continuum mechanics description upon approaching the molecular scale. A deviation from the Lamb model was observed experimentally on the breathing frequency of clusters from Au_{25} down to Au_{10} by TRS[20,25] but the frequency of the quadrupolar mode still seems to be consistent with Lamb theory down to 10 atoms of gold. All these studies have been performed with clusters electronically and structurally stabilized by ligands. At such small sizes the ligands most likely affect the vibrational and electronic properties of molecular clusters, as recently observed with atomically thin nanoplatelets[26,27] and small nanocrystals[28]. The few reports on the dynamics of grafted nanoparticles were mainly concerned with the inertial effect of the surface ligands, where these latter are not

dynamically involved in the core vibration. Unraveling the ligand contribution to the core dynamics at molecular sizes thus remains a major issue to be addressed in order to properly assess the vibrational spectra of atomic size clusters. In this work, we demonstrate the considerable role of ligands in the lattice dynamics of gold nanoclusters upon approaching the molecular size range. We report the observation of vibrational spectra of ligand-stabilized clusters Au_6 and Au_9 using LFRS. The experimental data are then confronted to the vibration frequencies computed using Density Functional Theory (DFT) and to the linear elasticity theory using the Lamb model with the Mass Load Approximation. Finally, we address the influence of the ligand's nature and the temperature on the vibrational dynamics on a Au_{25} cluster.

Methods

Nowadays, the remarkable progresses of chemical synthesis techniques allow to produce clusters presenting a highly monodispersed size distribution. In this work we have focused on three cluster sizes: Au_6, Au_9 and Au_{25}. They are respectively stabilized with, Bis(diphenylphosphino)propane (Dppp), Triphenylphosphine (PPh_3), 4-mercaptobenzoic acid, (p-MBA) and Gluthatione (SG) ligands, and have been prepared using different methods reported elsewhere[29–31] and briefly summarized in the supplementary information.

The monodispersity, in terms of the size of our clusters, has been characterized using optical absorption and mass spectroscopy (see Figure S2 and S3 in the Supporting Information). The Low Frequency Raman Spectroscopy experiment were carried out using a LabRAM HR spectrometer (HORIBA Jobin Yvon) operating with an excitation laser line at 532 nm. In all experiments, the signal was collected in backscattering geometry with a long-working distance objective (20× magnification). The scattered light was dispersed by a 1800 grooves/mm and inelastic signal can be detected down to about 6 cm^{-1}. This optical setup is compatible with our temperature controller

system (LINKAM) from -180°C to 100°C. Because of the atomically precise size distribution of the clusters, we assume that the Raman peaks are not significantly broadened by the size inhomogeneity contribution. Raman spectra were typically average ten times with an exposure time of 180 seconds and a power density around 10^6 mW/cm^2.

The clusters structures have been previously determined by X-ray crystallography for $Au_6(Dppp)_4(NO_3)_2$[29] and $Au_9(PPh_3)_8(NO_3)_3$[30]. The Au_6 geometry is based on a tetrahedron and two atoms are bonded to two edges without apex in common (inset Figure 1.A). The structure of Au_9 consists of a plan of five gold atoms while the four others are symmetrically distributed from either side from this plan (inset Figure 1.B). The structure of $Au_{25}(SG)_{18}$ has not yet been reported in the literature. Nevertheless, DFT calculations have shown that the geometry of Au_{25} cluster remains stable for numerous thiolate ligands[32]. As a matter of fact, we have supposed that structure of the gold core of $Au_{25}(SG)_{18}$ is similar to the $Au_{25}(SCH_2CH_2Ph)_{18}$ one, determined by X-ray diffraction[33]. The structure of Au_{25} present an icosahedral gold core (inset Figure 5.C) composed of 13 gold atoms and a shell with 12 stellated gold atoms bonded to 18 sulfur atoms.

DFT calculations were performed using the M06 DFT functional[34] integrated in the Gaussian 09 set of programs[35]. Initial geometries of $(Au_6(Dppp)_4)^{2+}$ and $(Au_9(PPh_3)_8)^{3+}$ have been taken from Alvino et al.[36]. The LanL2DZ basis set was employed for each atom[37–39]. Structural parameters result from full geometry optimization in the gas phase, with no imposed constraints and the convergence criterion was set up so that the maximum atomic force is negligible. The computation and further diagonalization of the Hessian matrix provides vibrational frequencies and eigenvectors.

The Mass Load model is based on the effect of an inertial mass on the surface of the nano objects influencing their vibration modes. This model has been previously developed to explain experimental deviations observed from the Lamb model in the case of thin nanoplatelets

chemically synthesized[26]. In this article, such reasoning has been applied to the case of three-dimensional resonators. The nano object is covered with ligands whose surface density ϱ_L is not negligible compared to the mass of the particle. Each cluster is defined by a gold sphere of radius R with its acoustic properties: the volumetric mass density ϱ_c=19.3 kg.m^{-3}, longitudinal and transverse sound velocities v_L=3330 m.s^{-1} and v_T=1250 m.s^{-1}, and the surface density ϱ_L is calculated from the molecular weight and the number of ligands on each cluster. The stress at the surface of the particle should no longer be assumed to be zero as in Lamb's model. The Mass Load model simply add to the Lamb's system of equations the terms of inertia of the surface depending on the surface density ϱ_L.

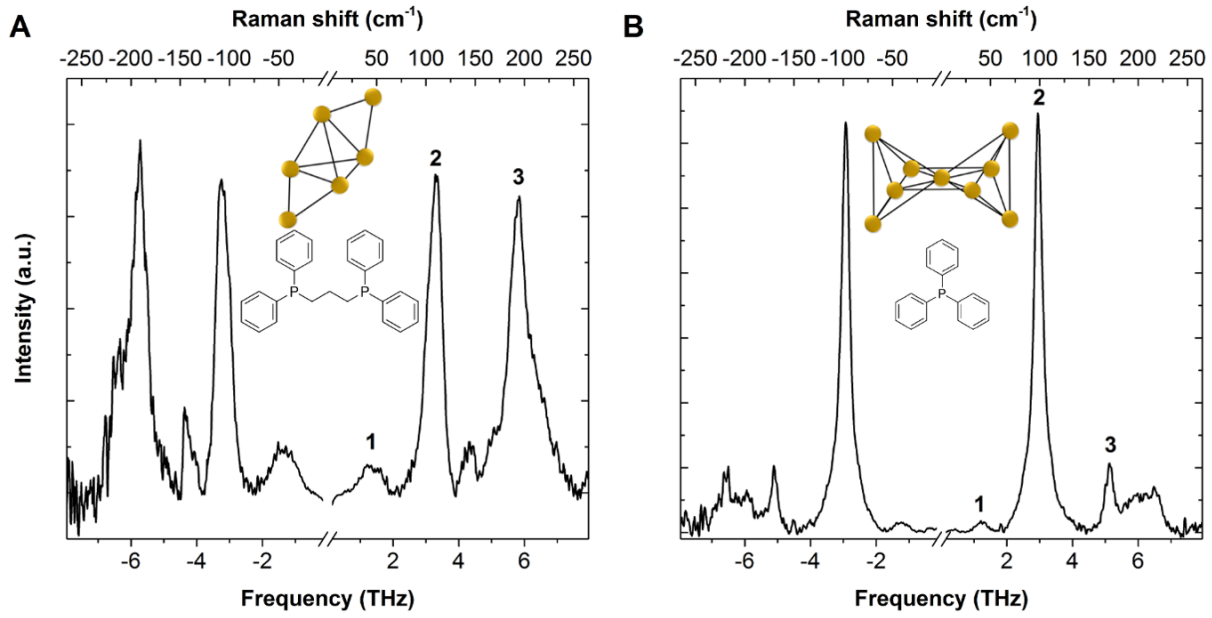

Figure 1. Low frequency Raman spectra of **A)** $[Au_6(Dppp)_4]^{2+}$ and of **B)** $[Au_9(PPh_3)_8]^{3+}$. Spectra have been measured at ambient temperature with an excitation at 532 nm. The abscissa scale is displayed using both frequencies (bottom) and wave numbers (top). In insets, structure of gold core and ligands of each clusters have been represented.

Results and Discussion

Background-corrected Raman spectra of $[Au_6(Dppp)_4]^{2+}$ and $[Au_9(PPh_3)_8]^{3+}$ clusters are displayed in Figure 1.A and 1.B**,** in which the Rayleigh line, due to the elastic scattering, has been removed for clarity. The spectra present several modes well separated: both $[Au_6(Dppp)_4]^{2+}$ and $[Au_9(PPh_3)_8]^{3+}$ have a large band (peak 1) centered around 1.34 THz and 1.24 THz, a peak (peak 2) at 3.37 THz and 2.95 THz and finally another peak (peak 3) at 5.79 THz and 5.13 THz respectively.

First, we need to separate the core and the ligand contributions to these vibrational spectra. In order to correctly assign the origin of each observed phonon for $[Au_6(Dppp)_4]^{2+}$ and $[Au_9(PPh_3)_8]^{3+}$ we have checked that the three Raman peaks survive above the ligand fusion at high temperature (T_{melt}(Dppp) = 338 K and T_{melt}(PPh_3) = 353 K), see details in the Supplementary Information S5 and S6. For these experiments, we followed the temperature evolution of the frequency of each labelled peak upon increasing the temperature from 77 K up to 373 K. The respective relative shifts of $[Au_6(Dppp)_4]^{2+}$and $[Au_9(PPh_3)_8]^{3+}$ clusters are, for peak 2, 2.5% and 3.3% and for peak 3, 1.3% and 3.5%. The width of peak 1 prevents a proper estimation of the slope of its temperature dependency. These relative shifts have to be compared to the temperature dependence of the acoustic vibration frequencies of both gold and ligands (Dppp and PPh_3)[40]. The temperature dependence of the elastic constants of gold allows us to estimate[41] the relative variation of the breathing and quadrupolar modes frequencies with temperature as :

$$\frac{d\nu_{l=0}}{\nu_{l=0}} = \frac{1}{2}\left(\frac{dC_{11}}{C_{11}} - \frac{d\rho}{\rho}\right) \; and \; \frac{d\nu_{l=2}}{\nu_{l=2}} = \frac{1}{2}\left(\frac{dC_{44}}{C_{44}} - \frac{d\rho}{\rho}\right)$$

Where C_{11} and C_{44} are the elastic stiffness coefficients and ϱ the density. These formulae provide an estimation of the relative frequency shift of 2.7% for the quadrupolar mode and 2.1% for the breathing mode, in good agreement with our LFRS result.

The elastic stiffness coefficient C_{11} of the ligands at different temperatures is deduced from the measure of the ultrasonic longitudinal acoustic velocity using Brillouin light scattering in the backscattering geometry. The obtained relative C_{11} shifts in the same temperature range are 22% and 21% for Dppp and PPh_3, way too high compared to those of $Au_6(Dppp)_4$ and $Au_9(PPh_3)_8$ Raman peaks. For this reason, we attribute the LFRS peaks 2 and 3 of both $Au_6(Dppp)_4$ and $Au_9(PPh_3)_8$ clusters to vibrational signature of the gold cores.

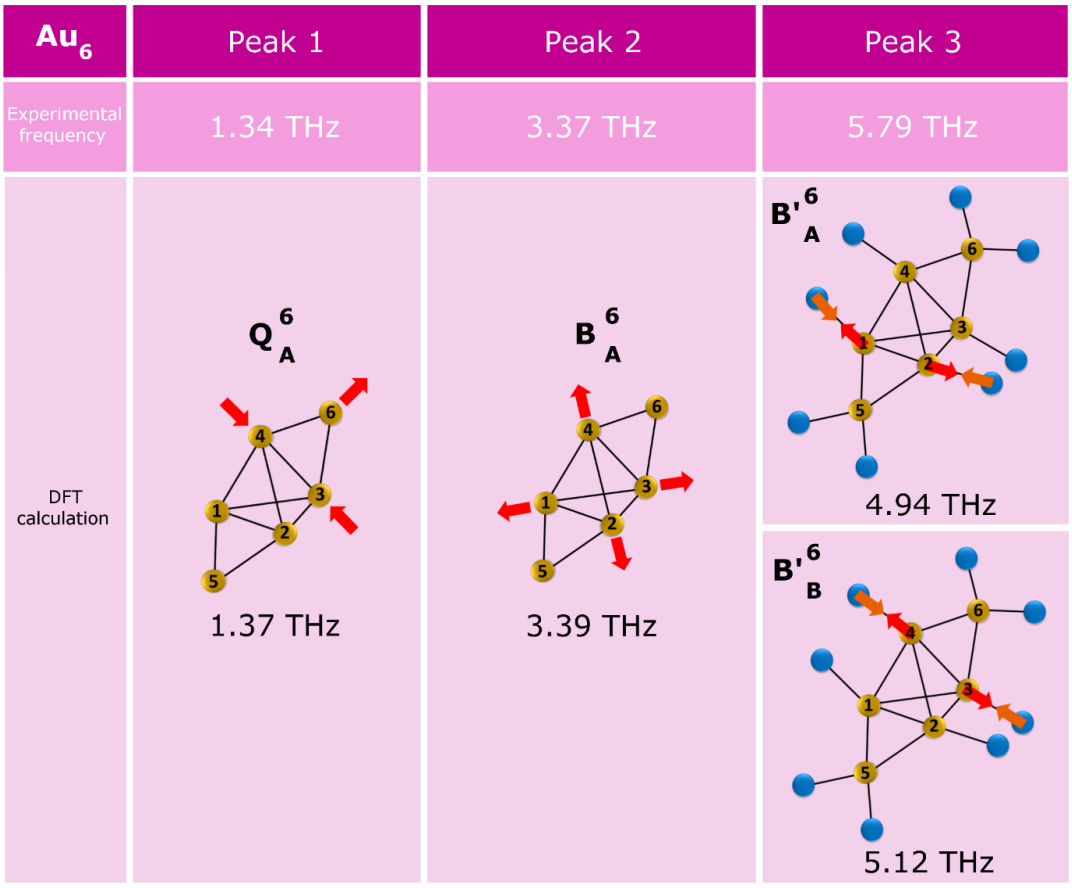

Figure 2. Schematic representation of gold atoms main displacements of DFT-computed vibration modes corresponding to peak 1, 2 and 3 for $[Au_6(Dppp)_4]^{2+}$. Below each sketch, the corresponding frequency obtained numerically is compared with the experimental frequency presented above. Each DFT computed mode is labelled by a name reported above each sketch. Yellow and blue

spheres correspond respectively to gold and phosphorus atoms. For peak 3, phosphorus atoms from ligands are represented as their displacement does not follow the one of gold atoms.

In order to further identify the vibration modes observed in the Raman spectra, DFT calculations have been performed to address the phonons frequencies and displacement eigenvector of $[Au_6(Dppp)_4]^{2+}$ and $[Au_9(PPh_3)_8]^{3+}$. Among all the modes that occur in this frequency range, we have selected the ones involving a noticeable displacement of the gold atoms and having a symmetry warranting a significant Raman activity (i.e. similar to the ones of quadrupolar and breathing Lamb modes).

We present in Figure 2 the displacement pattern and the experimental frequencies of the corresponding calculated vibration modes. In the case of $[Au_6(Dppp)_4]^{2+}$, peaks 1 (1.34 THz) and 2 (3.37 THz) were attributed to a quadrupolar-like mode of atoms 3, 4 and 6 at 1.37 THz (called Q^6_A) and a breathing-like mode (called B^6_A) of the tetrahedron (atoms 1, 2, 3 and 4) at 3.39 THz. We have not been able to identify a single calculated mode mainly involving gold atoms, likely to have a significant Raman activity in the vicinity of the experimental peak 3 (5.79 THz). However, from the DFT calculations, two presumably Raman active modes, B'^6_A and B'^6_B, exhibiting a significant displacement of gold atoms have been identified at smaller frequencies (4.94 THz and 5.12 THz). These modes correspond respectively to the stretching of bond 1-2 and 3-4 in opposite phase with the phosphorus atoms of the ligands.

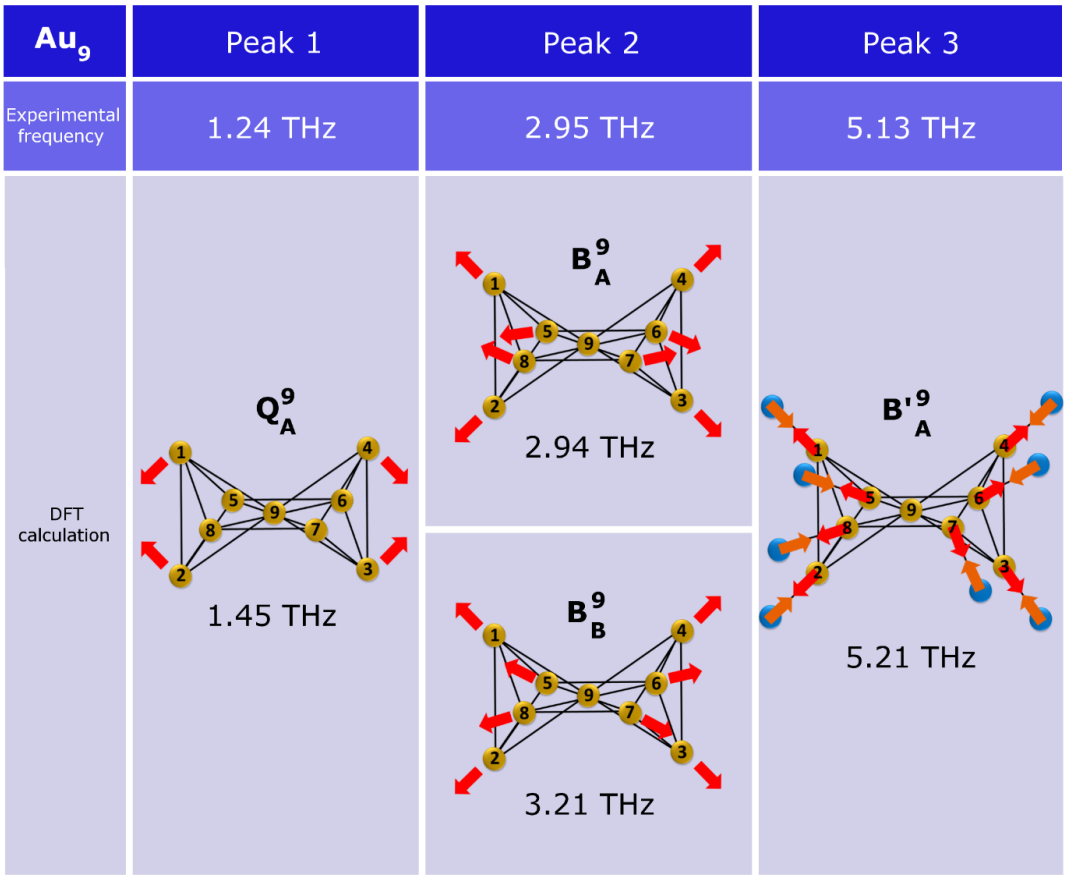

Figure 3. Schematic representation of gold atoms main displacements of DFT-computed vibration modes corresponding to peak 1, 2 and 3 for $[Au_9(PPh_3)_8]^{3+}$. Below each sketch, the corresponding frequency obtained numerically is compared with the experimental frequency presented above. Each DFT computed mode is labelled by a name reported above each sketch. Yellow and blue spheres correspond respectively to gold and phosphorus atoms. For peak 3, phosphorus atoms from ligands are represented as their displacement does not follow the one of gold atoms.

In the case of $[Au_9(PPh_3)_8]^{3+}$, DFT results are plotted in Figure 3. Experimental modes observed at 1.24 THz (peak 1), 2.95 THz (peak 2) and 5.13 THz (peak 3) have been attributed to the calculated modes respectively at 1.45 THz, (called Q^9_A), 2.94 THz (called B^9_A) and 5.21 THz (called B'^9_A). According to these results, peak 1 (1.24 THz) is a quadrupolar-like mode involving only atoms 1, 2, 3 and 4 in the Oxz plane, while the ligands follow a similar movement. Peak 2 (2.95

THz) corresponds to a breathing- like displacement of atoms 1, 2, 3 and 4 mixed with a quadrupolar-like movement of atoms 5,6, 7 and 8 in the Oxy plan. Another calculated mode called B^{9}_{B} (3.21 THz), involving a breathing-like displacement of all gold atoms and ligands, may also contribute to the experimental peak 2 (2.95 THz). For these two last modes, ligands follow the movement of gold atoms where they are grafted. Finally, peak 3 (5.13 THz) is attributed to a calculated mode at 5.21 THz, corresponding to a radial displacement of all gold atoms and ligands in an opposite phase relationship.

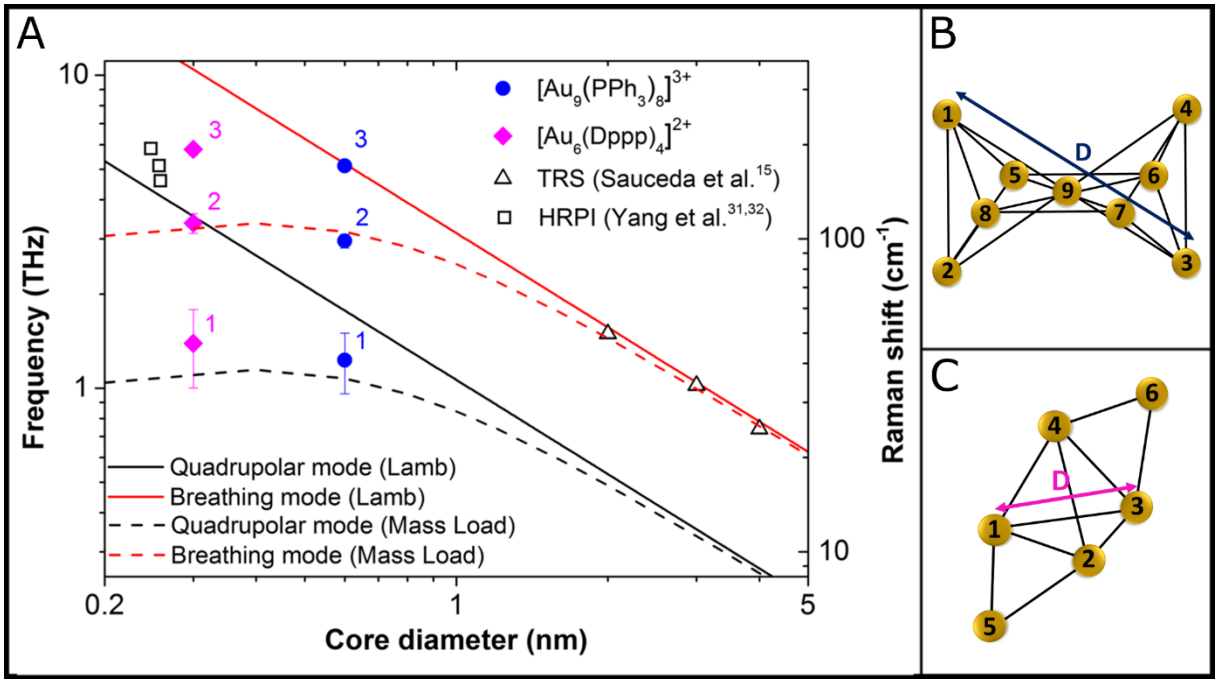

Figure 4. **A)** Acoustic mode vibration frequency as a function of the gold core diameter given in THz (left scale) and wavenumber (right scale). Experimental frequencies from the literature obtained by TRS (black triangles[14]), and by high resolution photoelectron imaging (HRPI, black squares[36,37]) and measurements done by LFRS in this study (pink diamonds $[Au_6(Dppp)_4]^{2+}$, blue circles $[Au_9(PPh_3)_8]^{3+}$). Black and red solid lines are respectively the theoretical quadrupolar (ℓ=2), breathing (ℓ=0) fundamental (n=1) frequencies of the gold cores, according to the Lamb theory.

Dashed lines are frequencies of the gold core obtained with the Mass Load model (considering a ligand layer of 0.6 nm thick with a density of 1.2g.cm^{-3}). **B)** and **C)** show the equivalent diameter for Au_9 and Au_6 respectively.

In order to probe the validity of the continuum elasticity laws at this molecular scale, we have compared the experimental Raman active modes frequencies with the ones computed using the Lamb model for the quadrupolar and breathing ℓ=2 and ℓ=0 modes. As we have demonstrated that, by changing the temperature, we probe the vibration of the gold core by LFRS, we will consider only the size of the gold core for Lamb Model. This last one relies also on the important assumption that the cluster geometry can be approximated by a sphere with a diameter D. Note that a recent time-resolved study has proved that the acoustic frequencies of molecular clusters with non-perfectly spherical shapes can be correctly calculated using Lamb model by considering a spherical rigid body in first approximation[15]. The core size is commonly estimated by calculations based on an FCC structure[25]. However, the atomic structure of Au_6 and Au_9 clusters being far from a FCC packing, we have defined the clusters diameters as the distances D displayed on Figure 4.B and 4.C by considering the gold atoms with a displacement in the modes calculated with DFT. The frequencies calculated using the Lamb model have been compared to the experimental ones in Figure 4 for $[Au_6(Dppp)_4]^{2+}$ (pink diamond) and $[Au_9(PPh_3)_8]^{3+}$ (blue sphere) clusters as a function of the estimated gold core diameter D. The frequencies of ℓ=2 (quadrupolar) and ℓ=0 (breathing) modes, given by the Lamb theory, are reported as solid black (ℓ=2) and red (ℓ=0) lines. As observed on this figure, the Lamb model applied to the gold core only, fails to reproduce the experimental results obtained for $[Au_6(Dppp)_4]^{2+}$ and $[Au_9(PPh_3)_8]^{3+}$. This failure appears also if we consider nanoplatelets or quantum dots where the low frequency vibrational modes deviate from the Lamb theory[26,42] and can be attributed to the absence of the ligand in the model. This effect

appears when the size of a nanoparticle is sufficiently small so that the masses of ligands and core are comparable. In order to address this case, we have included the effect of the ligand layer by modifying the boundary conditions in the Lamb model.

Here we have considered the Mass Load approach, detailed in the Methods section to estimate the effect of an additional inertial mass attached to the surface of the gold clusters. Within this approach, the gold core is loaded with a homogeneous inertial surface layer having the mass of the ligands. As an example, the Mass Load effect induces a 10% downshift of the Lamb frequency of quadrupolar and breathing modes when the ligand layer mass is a quarter of the core one. Mass-load corrected Lamb Frequencies are reported as dotted black line (ℓ=2) and red (ℓ=0) lines in Figure 4 as a function of the Au core diameter D for the quadrupolar-like and breathing-like modes respectively. Considering this additional inertial mass improves the prediction of the Lamb theory, especially regarding peaks 1 and 2 for both $[Au_6(Dppp)_4]^{2+}$ and $[Au_9(PPh_3)_8]^{3+}$. The quadrupolar character of peak 1 is confirmed for both $[Au_6(Dppp)_4]^{2+}$ and $[Au_9(PPh_3)_8]^{3+}$ and a breathing-like character is found for the Peak 2 mode, in agreement with DFT calculations for $[Au_6(Dppp)_4]^{2+}$. The attribution of the Peak 2 of $[Au_9(PPh_3)_8]^{3+}$ to a breathing mode by DFT is arguable because two calculated modes could correspond to Peak 2. However, among these two modes, one of them has clearly a breathing character. In the DFT calculations, another breathing mode of $[Au_9(PPh_3)_8]^{3+}$ has been attributed to the Peak 3. However, this calculated mode presents out-of-phase oscillations of the ligands and the gold core, analogous to the first harmonic of the breathing mode of a system containing the gold core and the ligands. Such mode can obviously not be explained by the Mass Load model applied on the gold core only. We have thus considered the dynamic behavior of the ligands-core bonds, the ligands being grafted to the gold core via a P-Au covalent bonds. When gold core oscillates, ligands can either follow the movement and load the surface of the cluster or

oscillate in opposite phase with the gold core. The Au-P bonding[43] is as strong as Au-Au bond[44] (both nearly 220 kJ.mol-1). The phosphorus layer can thus be considered as belonging to the core, yielding to a hybrid gold-phosphorus core with a diameter of 1.2 nm in the case of $[Au_9(PPh_3)_8]^{3+}$. Considering the mass load on this hybrid model, the frequency of the first harmonic of the breathing mode, 5.15 THz, is in good agreement with the experimental frequency of peak 3 (5.13 THz). Our results demonstrate that the Lamb model, completed by Mass Load approximation, remains a possible approach to predict the vibrational modes of gold quantum clusters as long as the ligands are considered. As no other work exists for such small size for metallic cluster stabilized by ligand we have to compare our results to those obtained without ligands. In that case, the measured vibrational mode frequency evolution with size is far from the Lamb model prediction: for the Au2 cluster[45], a vibration frequency of 5.82 THz was obtained from photoelectron imaging, which is very different from the Lamb theoretical breathing frequency of 10.38 THz. Moreover, this frequency is strongly shifted for the anionic Au_2^- cluster toward 4.59 THz. With similar experiment, study of Au_4 and Au_4^- clusters[46] present an analogous behavior. Given the lack of data concerning the bare Au_6 cluster, and since the combination of the Lamb theory and the Mass Load model succeeds in predicting the vibration modes of $[Au_6(Dppp)_4]^{2+}$, we suspect that the role played by the ligands is thus crucial regarding the reliability of the Lamb model for such small clusters. The coordination number of gold atoms in bare Au_2 and Au_4 clusters[45,46], not stabilized by ligands, is very low (between 1 to 3), in contrast to gold atoms of ligand-stabilized clusters presented in this work (between 4 to 8). In these latter, due to the presence of ligands, electronic environment of the gold atoms and thus elastic properties are then closest to that of the bulk. Aiming to refine our understanding of the effect of the ligand on the elastic properties of cluster, we have studied how the ligand bonding influences the vibrational spectrum

of the metallic cluster. We chose to work with Au_{25} core. This latter is sufficiently large to minimize inertial effect and its ligands can be exchanged, retaining the core structure.

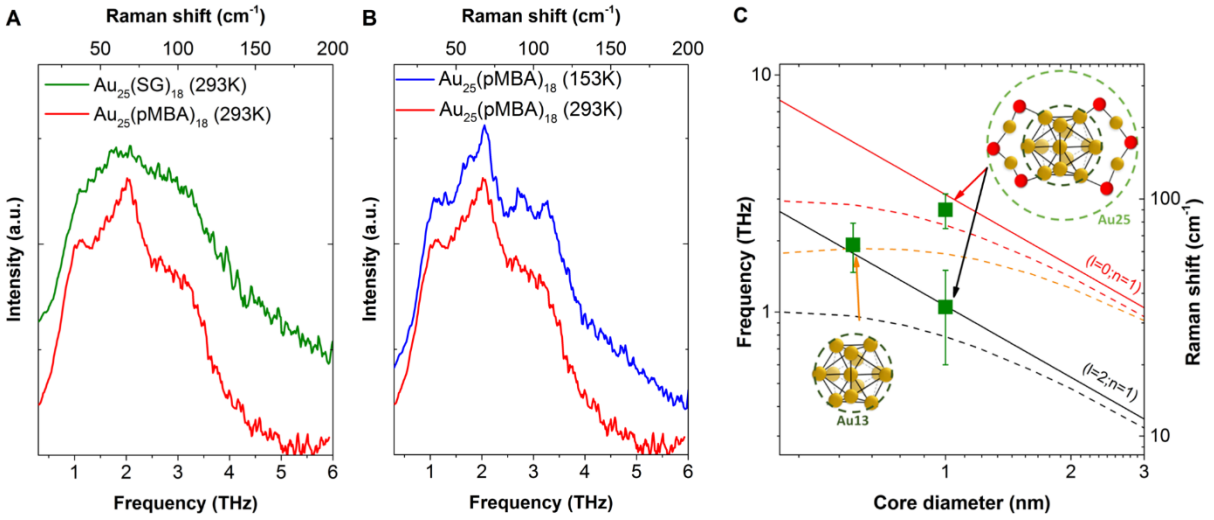

Figure 5. A) LFRS of $Au_{25}(SG)_{18}$ (green line) and Au_{25}(p-MBA)$_{18}$ (red line) at ambient temperature and **B)** LFRS of Au_{25}(p-MBA)$_{18}$ at 293K (red line) and at 153K (blue line) with an excitation at 532nm. **C)** Experimental frequencies (green squares) as a function of the gold core diameter, measured in this work for $Au_{25}(SG)_{18}$. Black and red solid lines are respectively the theoretical quadrupolar (ℓ=2), breathing (ℓ=0) fundamental (n=1) frequencies of the gold cores, according to the Lamb theory. Black and red dashed lines correspond the mass load corrected Lamb model. The orange dashed line corresponds to the breathing mode of a Au_{13} core with a Mass Load correction involving both the ligands and the twelve stellated gold atoms.

We have investigated the vibrational properties of Au_{25} capped with two different ligands: one aliphatic (Glutathione, referred as SG) and one aromatic (4-mercaptobenzoic acid, referred as p-MBA). In these clusters, $Au_{25}(SG)_{18}$ and Au_{25}(p-MBA)$_{18}$, the ligands are attached to the core through gold-sulfur bonds. LFRS of dry powders of $Au_{25}(SG)_{18}$ and Au_{25}(p-MBA)$_{18}$ at ambient temperature

are presented in Figure 5.A. For $Au_{25}(SG)_{18}$ clusters, we observe a large band from 0.3 to 6 THz which presents a barely visible sub-structuration. This structure is better resolved for Au_{25}(p-MBA)$_{18}$ clusters and seems to be constituted with three modes at 1.1, 1.9 and 2.7 THz (±0.4 THz). Unfortunately, the exact nature of these modes cannot be investigated using DFT calculations. Indeed, available experimental data reporting the geometry of the Au_{25}(p-MBA)$_{18}$ cluster are missing in the literature. The determination of the equilibrium configuration of the grafted cluster would require a global exploration of the DFT potential energy landscape, which is out of our computational capabilities. Recent work has been realized on the same clusters with alternative ligands in liquid phase using TRS[25]. Two modes observed at 1.2 ± 0.2 THz and 2.4 ± 0.3 THz were attributed to the quadrupolar and breathing modes of the cluster. These TRS experimental results can be compared to our LFRS experiment. The TRS peaks at 1.2 THz and 2.4 THz are respectively consistent with the LFRS peaks at 1.1 THz and 2.7 THz. Figure 5.C shows the vibration frequencies from the Lamb (solid lines) and the mass load models (dashed lines) for the breathing (ℓ=0) and the quadrupolar (ℓ=2) modes. For the peaks at 1.1 and 2.7 THz, experimental LFRS measurements (green squares) agree with both Lamb and mass load models and correspond respectively to quadrupolar and breathing modes[25]. In this latter, the core contains 25 atoms and the load mass involves the 18 SG ligands. Concerning the peak at 1.9 THz, it cannot be explained with a 25-atoms core. We have interpreted this intermediate mode using the Mass Load model, as a breathing mode of the icosahedral core Au_{13} with a load mass corresponding to both the 18 SG ligands and the 12 stellated gold atoms (orange dashed line on Figure 5.C). Indeed, in the structure reported in ref 31, the Au_{25} core contains a well-defined icosahedral Au_{13} core and 12 stellated gold atoms strongly bonded to the sulfur atoms of ligands and weakly bonded to the Au core atoms. We

can conclude that molecular description of cluster, i.e atomic arrangement, turns out to be crucial to interpret properly vibration spectra.

We consider now the effect of the ligands upon the vibration modes of Au_{25} cluster. No significant mass load shift in frequencies is observed between $Au_{25}(SG)_{18}$ and Au_{25}(p-MBA)$_{18}$, but it appears that the peak width and the intensity of each mode are different. Indeed, with p-MBA as ligands, the intermediate mode, associated to the icosahedral core, has a little higher energy shift and a quality factor higher compared to the one obtained with SG ligands. SG and p-MBA ligands are fixed to the metallic cluster by Au-S covalent bonding to the gold core. The Au-S bond between ligand and core is stronger for the aliphatic SG than for the aromatic p-BMA[47]. In the former case, the ligand-core bond is thus more similar to the Au-Au bonding within the core. The core-ligand bonding can be seen as the limit between core and ligands. If the coupling is weak, in our case with p-MBA, confinement of the vibration of the core is better and the damping lower. On the opposite hand, with SG ligand, the coupling is stronger and the confinement is smaller, the quality factor is then lower and the energy of the vibration is also lower. This structural difference of the ligand layer induces that the p-MBA affects less the vibration of the inner core which is less strained. The quality factor of the vibration mode of the inner core is then higher with ligands less strongly bonded, in our case with p-MBA. We can conclude that at ambient temperature the ligands have a large impact on the quality factor of the vibrational resonances thanks to their bonds to the core.

In order to better distinguish these modes, we choose to reduce the temperature of the system. In this way, the modes amplitude is reduced and thus the non-linear coupling between vibrational modes inside the cluster is also smaller, inducing a reduced damping and an increased quality factor. Results obtained with Au_{25}(p-MBA)$_{18}$ cluster at 153 K and at 293 K are presented in Figure 5.B. A sub-structuration of the three Lamb modes observed at ambient temperature starts to be

distinguished at 153 K. The two breathing modes, attributed to Au_{13} and Au_{25} structures, both presents at least two contributions, respectively at 1.7 and 2.1 THz and 2.8 and 3.2 THz. The Lamb model considering a spherical nanoparticle cannot explain this separation of the breathing mode into several structures. This difference can be explained by considering the molecular structure and anisotropic properties of the $Au_{25}(p\text{-}MBA)_{18}$ cluster. For comparison, according to DFT calculations for the $[Au_9(PPh_3)_8]^{3+}$ cluster, two modes exist at 2.94 THz (B^9_B) 3.21 THz (B^9_A)**,** but are not resolved in the experimental spectrum (see Figure.1.B). The separation of vibrational modes is an effect of the loss of spherical symmetry due to the discretization of matter. With so few atoms, it is not possible to consider a perfectly isotropic and spherical cluster. However, the resulting anisotropic mechanical properties of the aggregate are difficult to determine. By considering the shape of the cluster, these two effects produce a degeneration of the natural modes of vibration. As shown in the case of $[Au_9(PPh_3)_8]^{3+}$, these same modes are more easily calculated using DFT. Thus, the evolution of the low-frequency Raman spectrum with a decrease in temperature illustrates the transition from a continuous model description to a molecular one for the vibrational modes of clusters. At room temperature, the $Au_{25}(p\text{-}MBA)_{18}$ spectrum is described by Lamb theory while at low temperature, the increase in quality factors reveals a substructure that cannot simply be interpreted with the approximation of the isotropic sphere of the Lamb model.

Conclusions

In summary, Low Frequency Raman Spectroscopy measurements were performed on grafted Au_6, Au_9 and Au_{25} clusters. Experimental vibrations frequencies of the Au_6 and Au_9 clusters were compared to DFT calculations and predictions of the Lamb Model. It appears that this latter continuum mechanics model, corrected by the mass effect, still works to predict quadrupolar-like

and breathing-like modes down to 6-atom clusters stabilized by ligands. We attribute this surprising adequacy to the presence of ligands which maintains high degrees of coordination of gold atoms. For largest cluster Au_{25} we have probed the effect of the ligands and the temperature on vibrational modes. Quadrupolar and breathing modes have frequencies in good agreement with the Lamb theory. An additional observed mode is attributed to the breathing vibration of the icosahedral Au_{13} nucleus. It appears that the nature of bonding with the ligands also affects the confinement of the gold vibration by changing the coupling between the core and the ligand. This work demonstrates that the elasticity defined in continuum mechanics, on which Lamb's theory is based, remains suitable to describe vibrations of such small decorated gold clusters, provided the use of the mass load approximation. As this last correction seems not sufficient to explain the sub-structuration, observed only at low temperature inside the large bands of Au_{25}(p-MBA)$_{18}$ spectrum, we can question the approximation which consists in considering aggregates as homogeneous nanospheres. If we want to probe more precisely the performance of the Lamb approach we have to propose a more realistic description of the cluster. But, inevitably, the exact knowledge of the aggregate/ligand shape and energies of each bonding, which are essential to achieve this goal, is not yet computable for Au_{25} aggregates. Beyond this study of gold clusters decorated by thiolates, the quantitative determination of the relative effect of the ligand mass and of the Au-ligand interaction strength on the structure of the aggregates and so on their vibration modes would allow a better understanding of the spread of validity of continuum mechanics.

SUPPORTING INFORMATION

Cluster synthesis protocols, UV-Visible Absorption and Mass Spectroscopy spectra of clusters, Temperature dependency of Low Frequency Raman spectra for $[Au_9(PPh_3)_8]^{3+}$ and $[Au_6(dppp)_4]^{2+}$ clusters and their ligands, Low Frequency Raman spectra of PPh_3 and dppp.

AUTHOR INFORMATION

Corresponding Author : * Quentin Martinet : E-mail qumartinet@ucsd.edu

* Alice Berthelot : E-mail alice.berthelot@univ-lyon1.fr

Present Address : ¶ Department of Physics, University of California, San Diego, USA

ACKNOWLEDGMENT

We acknowledge C. Clavier, G. Cagnoli. This work has been done thanks to the support of the CECOMO platform of the University of Lyon. This work was granted access to the HPC resources of CALMIP supercomputing center under the allocation p1303.

REFERENCES

(1) Li, X.-B.; Wang, H.-Y.; Yang, X.-D.; Zhu, Z.-H.; Tang, Y.-J. Size Dependence of the Structures and Energetic and Electronic Properties of Gold Clusters. *J. Chem. Phys.* **2007**, *126*, 084505.

(2) Russier-Antoine, I.; Bertorelle, F.; Vojkovic, M.; Rayane, D.; Salmon, E.; Jonin, C.; Dugourd, P.; Antoine, R.; Brevet, P.-F. Non-Linear Optical Properties of Gold Quantum Clusters. The Smaller the Better. *Nanoscale* **2014**, *6*, 13572–13578.

(3) Bayle, M.; Combe, N.; Sangeetha, N. M.; Viau, G.; Carles, R. Vibrational and Electronic Excitations in Gold Nanocrystals. *Nanoscale* **2014**, *6*, 9157–9165.

(4) Oliver-Meseguer, J.; Cabrero-Antonino, J. R.; Dominguez, I.; Leyva-Perez, A.; Corma, A. Small Gold Clusters Formed in Solution Give Reaction Turnover Numbers of 107 at Room Temperature. *Science* **2012**, *338*, 1452–1455.

(5) Jortner, J. Cluster Size Effects. *Z Phys D - Atoms, Molecules and Clusters* **1992**, *24*, 247–275.

(6) Chou, M. Y.; Cohen, M. L. Electronic Shell Structure in Simple Metal Clusters. *Physics Letters A* **1986**, *113*, 420–424.
(7) Martin, T. P.; Bergmann, T.; Goehlich, H.; Lange, T. Shell Structure of Clusters. *J. Phys. Chem.* **1991**, *95*, 6421–6429.
(8) Malola, S.; Lehtovaara, L.; Enkovaara, J.; Häkkinen, H. Birth of the Localized Surface Plasmon Resonance in Monolayer-Protected Gold Nanoclusters. *ACS Nano* **2013**, *7*, 10263–10270.
(9) Campos, A.; Troc, N.; Cottancin, E.; Pellarin, M.; Weissker, H.-C.; Lermé, J.; Kociak, M.; Hillenkamp, M. Plasmonic Quantum Size Effects in Silver Nanoparticles Are Dominated by Interfaces and Local Environments. *Nat. Phys.* **2019**, *15*, 275–280.
(10) Sun, C. Q. Size Dependence of Nanostructures: Impact of Bond Order Deficiency. *Progress in Solid State Chemistry* **2007**, *35*, 1–159.
(11) Tanguy, A.; Wittmer, J. P.; Leonforte, F.; Barrat, J.-L. Continuum Limit of Amorphous Elastic Bodies: A Finite-Size Study of Low-Frequency Harmonic Vibrations. *Phys. Rev. B* **2002**, *66*, 174205.
(12) Buck, U.; Krohne, R. Surface Vibrations from Small Clusters to the Solid: He Atom Scattering from Ar n. *Phys. Rev. Lett.* **1994**, *73*, 947–950.
(13) Del Fatti, N.; Voisin, C.; Chevy, F.; Vallée, F.; Flytzanis, C. Coherent Acoustic Mode Oscillation and Damping in Silver Nanoparticles. *The Journal of Chemical Physics* **1999**, *110*, 11484–11487.
(14) Lamb, H. On the Vibrations of an Elastic Sphere. *Proceedings of the London Mathematical Society* **1881**, *s1-13* (1), 189–212.
(15) Sauceda, H. E.; Mongin, D.; Maioli, P.; Crut, A.; Pellarin, M.; Del Fatti, N.; Vallée, F.; Garzón, I. L. Vibrational Properties of Metal Nanoparticles: Atomistic Simulation and Comparison with Time-Resolved Investigation. *J. Phys. Chem. C* **2012**, *116*, 25147–25156.
(16) Tlahuice-Flores, A.; Whetten, R. L.; Jose-Yacaman, M. Vibrational Normal Modes of Small Thiolate-Protected Gold Clusters. *J. Phys. Chem. C* **2013**, *117*, 12191–12198.
(17) Ruijgrok, P. V.; Zijlstra, P.; Tchebotareva, A. L.; Orrit, M. Damping of Acoustic Vibrations of Single Gold Nanoparticles Optically Trapped in Water. *Nano Lett.* **2012**, *12*, 1063–1069.
(18) van Dijk, M. A.; Lippitz, M.; Orrit, M. Detection of Acoustic Oscillations of Single Gold Nanospheres by Time-Resolved Interferometry. *Phys. Rev. Lett.* **2005**, *95*, 267406.
(19) Miller, S. A.; Womick, J. M.; Parker, J. F.; Murray, R. W.; Moran, A. M. Femtosecond Relaxation Dynamics of Au25L18–Monolayer-Protected Clusters. *J. Phys. Chem. C* **2009**, *113*, 9440–9444.
(20) Varnavski, O.; Ramakrishna, G.; Kim, J.; Lee, D.; Goodson, T. Optically Excited Acoustic Vibrations in Quantum-Sized Monolayer-Protected Gold Clusters. *ACS Nano* **2010**, *4*, 3406–3412.
(21) Juvé, V.; Crut, A.; Maioli, P.; Pellarin, M.; Broyer, M.; Del Fatti, N.; Vallée, F. Probing Elasticity at the Nanoscale: Terahertz Acoustic Vibration of Small Metal Nanoparticles. *Nano Lett.* **2010**, *10*, 1853–1858.
(22) Haslett, T. L.; Bosnick, K. A.; Moskovits, M. Ag5 Is a Planar Trapezoidal Molecule. *The Journal of Chemical Physics* **1998**, *108*, 3453–3457.
(23) Bosnick, K. A.; Haslett, T. L.; Fedrigo, S.; Moskovits, M.; Chan, W.-T.; Fournier, R. Tricapped Tetrahedral Ag7: A Structural Determination by Resonance Raman Spectroscopy and Density Functional Theory. *The Journal of Chemical Physics* **1999**, *111*, 8867–8870.

(24) Portales, H.; Saviot, L.; Duval, E.; Fujii, M.; Hayashi, S.; Del Fatti, N.; Vallée, F. Resonant Raman Scattering by Breathing Modes of Metal Nanoparticles. *The Journal of Chemical Physics* **2001**, *115*, 3444–3447.
(25) Maioli, P.; Stoll, T.; Sauceda, H. E.; Valencia, I.; Demessence, A.; Bertorelle, F.; Crut, A.; Vallée, F.; Garzón, I. L.; Cerullo, G.; Del Fatti, N. Mechanical Vibrations of Atomically Defined Metal Clusters: From Nano- to Molecular-Size Oscillators. *Nano Lett*. **2018**, *18*, 6842–6849.
(26) Girard, A.; Saviot, L.; Pedetti, S.; Tessier, M. D.; Margueritat, J.; Gehan, H.; Mahler, B.; Dubertret, B.; Mermet, A. The Mass Load Effect on the Resonant Acoustic Frequencies of Colloidal Semiconductor Nanoplatelets. *Nanoscale* **2016**, *8*, 13251–13256.
(27) Devkota, T.; Yu, K.; Hartland, G. V. Mass Loading Effects in the Acoustic Vibrations of Gold Nanoplates. *Nanoscale* **2019**, *11*, 16208–16213.
(28) Mork, A. J.; Lee, E. M. Y.; Dahod, N. S.; Willard, A. P.; Tisdale, W. A. Modulation of Low-Frequency Acoustic Vibrations in Semiconductor Nanocrystals through Choice of Surface Ligand. *J. Phys. Chem. Lett*. **2016**, *7*, 4213–4216.
(29) Van der Velden, J. W. A.; Bour, J. J.; Steggerda, J. J.; Beurskens, P. T.; Roseboom, M.; Noordik, J. H. Gold Clusters. Tetrakis[1,3-Bis(Diphenylphosphino)Propane]Hexagold Dinitrate: Preparation, x-Ray Analysis, and Gold-197 Moessbauer and Phosphorus-31{proton} NMR Spectra. *Inorg. Chem*. **1982**, *21*, 4321–4324.
(30) Wen, F.; Englert, U.; Gutrath, B.; Simon, U. Crystal Structure, Electrochemical and Optical Properties of [Au9(PPh3)8](NO3)3. *Eur. J. Inorg. Chem*. **2008**, *2008*, 106–111.
(31) Bertorelle, F.; Russier-Antoine, I.; Comby-Zerbino, C.; Chirot, F.; Dugourd, P.; Brevet, P.-F.; Antoine, R. Isomeric Effect of Mercaptobenzoic Acids on the Synthesis, Stability, and Optical Properties of Au25 (MBA)18 Nanoclusters. *ACS Omega* **2018**, *3*, 15635–15642.
(32) Tlahuice-Flores, A.; Whetten, R. L.; Jose-Yacaman, M. Ligand Effects on the Structure and the Electronic Optical Properties of Anionic Au25 (SR)18 Clusters. *J. Phys. Chem. C* **2013**, *117*, 20867–20875.
(33) Heaven, M. W.; Dass, A.; White, P. S.; Holt, K. M.; Murray, R. W. Crystal Structure of the Gold Nanoparticle [N(C8H17)4][Au25(SCH2CH2Ph)18]. *J. Am. Chem. Soc*. **2008**, *130*, 3754–3755.
(34) Zhao, Y.; Truhlar, D. G. The M06 Suite of Density Functionals for Main Group Thermochemistry, Thermochemical Kinetics, Noncovalent Interactions, Excited States, and Transition Elements: Two New Functionals and Systematic Testing of Four M06-Class Functionals and 12 Other Functionals. *Theor Chem Account* **2008**, *120*, 215–241.
(35) Frisch, M.; Trucks, G.; Schlegel, H.; Scuseria, G.; Robb, M.; Cheeseman, J.; Scalmani, G.; Barone, V.; Mennucci, B.; Petersson, G., et al. Gaussian 09, Rev. D. 01, Gaussian. *Inc., Wallingford, CT* **2009**.
(36) Alvino, J. F.; Bennett, T.; Anderson, D.; Donoeva, B.; Ovoshchnikov, D.; Adnan, R. H.; Appadoo, D.; Golovko, V.; Andersson, G.; Metha, G. F. Far-Infrared Absorption Spectra of Synthetically-Prepared, Ligated Metal Clusters with Au6, Au8, Au9 and Au6Pd Metal Cores. *RSC Adv*. **2013**, *3*, 22140-22149.
(37) Hay, P. J.; Wadt, W. R. Ab Initio Effective Core Potentials for Molecular Calculations. Potentials for K to Au Including the Outermost Core Orbitals. *The Journal of Chemical Physics* **1985**, *82*, 299–310.

(38) Hay, P. J.; Wadt, W. R. Ab Initio Effective Core Potentials for Molecular Calculations. Potentials for the Transition Metal Atoms Sc to Hg. *The Journal of Chemical Physics* **1985**, *82*, 270–283.
(39) Wadt, W. R.; Hay, P. J. Ab Initio Effective Core Potentials for Molecular Calculations. Potentials for Main Group Elements Na to Bi. *The Journal of Chemical Physics* **1985**, *82*, 284–298.
(40) Girard, A.; Gehan, H.; Crut, A.; Mermet, A.; Saviot, L.; Margueritat, J. Mechanical Coupling in Gold Nanoparticles Supermolecules Revealed by Plasmon-Enhanced Ultralow Frequency Raman Spectroscopy. *Nano Lett.* **2016**, *16*, 3843–3849.
(41) Neighbours, J. R.; Alers, G. A. Elastic Constants of Silver and Gold. *Phys. Rev.* **1958**, *111*, 707–712.
(42) Lee, E. M. Y.; Mork, A. J.; Willard, A. P.; Tisdale, W. A. Including Surface Ligand Effects in Continuum Elastic Models of Nanocrystal Vibrations. *J. Chem. Phys.* **2017**, *147*, 044711.
(43) Yu, H.; Liu, D.; Dang, Z.; Wang, D.; Fu, Y. Accurate Prediction of Au-P Bond Strengths by Density Functional Theory Methods. *Chin. J. Chem.* **2013**, *31*, 200–208.
(44) Luo, Y.-R. *Comprehensive Handbook of Chemical Bond Energies*, 1st ed.; CRC Press, 2007.
(45) León, I.; Yang, Z.; Wang, L.-S. High Resolution Photoelectron Imaging of Au2 –. *J. Chem. Phys.* **2013**, *138*, 184304.
(46) Yang, Z.; Leon, I.; Wang, L.-S. Communication: Vibrational Spectroscopy of Au4 from High Resolution Photoelectron Imaging. *J. Chem. Phys.* **2013**, *139*, 021106.
(47) Salvarezza, R. C.; Carro, P. The Electrochemical Stability of Thiols on Gold Surfaces. *Journal of Electroanalytical Chemistry* **2018**, *819*, 234–239.

TOC GRAPHIC